Intrinsic Tryptophan Fluorescence Identifies Specific Conformational Changes at the Actomyosin Interface upon Actin Binding and ADP Release†

C. M. Yengo, L. Chrin, A. S. Rovner, and C. L. Berger*

Department of Molecular Physiology and Biophysics, College of Medicine, University of Vermont, Burlington, Vermont 05405

Received May 28, 1999; Revised Manuscript Received August 4, 1999

ABSTRACT: The helix−loop−helix (A-site) and myopathy loop (R-site) are located on opposite sides of the cleft that separates the proposed actin-binding interface of myosin. To investigate the structural features of the A- and R-sites, we engineered two mutants of the smooth muscle myosin motor domain with the essential light chain (MDE), containing a single tryptophan located either in the A-site (W546-MDE) or in the R-site (V413W MDE). W546- and V413W-MDE display actin-activated ATPase and actin-binding properties similar to those of wild-type MDE. The steady-state fluorescence properties of W546-MDE [emission peak (λ_{max}) = 344, quantum yield = 0.20, and acrylamide bimolecular quenching constant (k_q) = 6.4 M^{-1}·ns^{-1}] and V413W-MDE [λ_{max} = 338, quantum yield = 0.27, and k_q = 3.6 M^{-1}·ns^{-1}] demonstrate that Trp-546 and Trp-413 are nearly fully exposed to solvent, in agreement with the crystallographic data on these residues. In the presence of actin, Trp-546 shifts to a more buried environment in both the ADP-bound and nucleotide-free (rigor) actomyosin complexes, as indicated by an average λ_{max} of 337 or 336 nm, respectively, and protection from dimethyl(2-hydroxy-5-nitrobenzyl)sulfonium bromide (DHNBS) oxidation. In contrast, Trp-413 has a single conformation with an average λ_{max} of 338 nm in the ADP-bound complex, but in the rigor complex it is 50% more accessible to DHNBS oxidation and can adopt a range of possible conformations (λ_{max} = 341−347 nm). Our results suggest a structural model in which the A-site remains tightly bound to actin and the R-site adopts a more flexible and solvent-exposed conformation upon ADP release.

Understanding the molecular mechanism of muscle contraction requires structural information about the specific interactions that occur between the motor protein myosin and polymeric actin. The crystal structure of the motor domain of myosin, which contains the nucleotide and actin-binding regions, has been solved from four different sources and in several nucleotide states (*1*−*6*). In addition, the crystal structure of monomeric actin (*7*−*9*) has been solved and used to construct a structural model of filamentous actin (F-actin) from electron density maps of F-actin (*10*). Since it has not been possible to crystallize the complex formed between actin and myosin, cryoelectron microscopy (cryo-EM) techniques have been used to reveal the overall conformation of the complex, as well as potential sites of interaction (*11*, *12*). However, it is still unclear which specific sites in myosin interact with actin or how these sites alter their conformation to cause changes in actin affinity and allow progression through the contractile cycle.

The available structural data on myosin and actin, as well as biochemical studies, have provided several clues as to which residues of myosin may participate in actin binding. One model suggests three regions of myosin (highlighted in Figure 1) that are important for the interaction with actin and provides a structural basis for the progression from weakly to strongly bound actomyosin complexes (*12*). Myosin subfragment 1 has historically been mapped by trypsin cleavage into an N-terminal 25 kDa fragment, a central 50 kDa fragment, and a C-terminal 20 kDa fragment. Two of the actin-binding sites proposed in the model, the A-site (purple) and the R-site (red), are separated by a large cleft (actin-binding cleft) that divides the 50 kDa tryptic fragment into the upper and lower 50 kDa subdomains, and a third region, the actin-binding loop (ABL) (cyan), connects the 50 and 20 kDa tryptic fragments (all residues refer to the smooth muscle myosin sequence unless indicated otherwise). First, it is predicted that the positively charged ABL (residues 628−657) forms electrostatic interactions with the negatively charged N-terminus of actin, allowing the transition from weakly (ATP and ADP−P_i) to strongly bound (ADP and nucleotide-free or rigor) states. This proposal is consistent with the results of cross-linking (*13*), proteolysis (*14*), and mutagenesis studies (*15*, *16*). Second, the A-site (residues 531−561), a helix−loop−helix structure on the lower 50 kDa subdomain, is thought to mediate formation of the strongly bound complex by forming hydrophobic contacts with actin in subdomain 4 (residues 338−348) (*12*). We have previously demonstrated that Trp-546, located in the A-site between two other hydrophobic residues (Cys-545 and Phe-547), shifts from a highly polar to a nonpolar environment in the presence of actin, suggesting that it participates in binding to actin in the strongly bound actomyosin complex (*17*). Third, the R-site (residues 406−416), an exposed loop on the upper 50 kDa subdomain that

† This work was supported by grants to C.L.B. from the NIH (AR44219) and AHA (96014500) and to A.S.R. from the AHA (95014630).

* To whom correspondence should be addressed: phone 802-656-0832; fax 802-656-0747; e-mail berger@salus.med.uvm.edu.

10.1021/bi991226l CCC: $18.00
Published on Web 10/14/1999

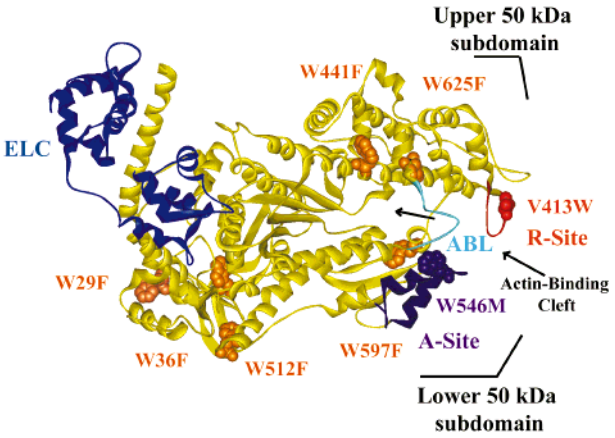

FIGURE 1: Crystal structure of the smooth muscle myosin motor domain essential light chain construct (MDE) with the myosin heavy chain (residues 1−819) colored yellow and the essential light chain colored blue (adapted from ref *1*). Also, the three putative actin-binding sites are labeled: the actin-binding loop (ABL) (residues 628−657) in cyan, the A-site (residues 531−561) in purple, and the R-site (residues 406−416) or myopathy loop in red. Six of the seven endogenous tryptophans, highlighted in orange, were substituted with phenylalanine, leaving a single endogenous tryptophan at residue 546 in the A-site (546-MDE). In addition, a second mutant containing a single tryptophan at residue 413 in the R-site was generated by substituting tryptophan 546 (purple space-filling model) with methionine and replacing valine 413 (red space-filling model) with tryptophan.

contains several charged and hydrophobic residues, is thought to interact with the C-terminus of actin to complete formation of the rigor complex (*12*). The R-site is also referred to as the myopathy loop, since a mutation within the loop (Arg403Glu) in β-cardiac myosin results in the deadly human disease familial hypertrophic cardiomyopathy (FHC)[1] (*18*). Indirect evidence, including synthetic peptides of the R-site that reduce the maximal actin-activated ATPase rate (V_{max}) of myosin without altering the K_M value (*19*) and phosphorylation of a serine/threonine residue in the R-site of nonmuscle myosins that increases the actin-activated ATPase activity dramatically (*20*, *21*), suggests that the R-site may mediate the affinity of myosin for actin. Thus, examining the structural properties of the R-site in the presence of actin may help to determine the role this loop plays in actin binding and identify the defect in FHC that disrupts motor function.

Obtaining structural information about domain motions within myosin during its interaction with actin has proven to be quite difficult. Several fluorescence studies have utilized exogenous labeling of the regulatory light chain (RLC) to demonstrate key structural rearrangements in the light chain-binding region in contracting muscle fibers, suggesting that it may function as a lever arm during force generation (reviewed in ref *22*). In addition, electron paramagnetic resonance has demonstrated a 30° rotation of the lever arm region (*23*) and a disordered to ordered change in the motor domain during muscle contraction (*24*, *25*). Interestingly, cryo-EM studies have revealed that smooth muscle myosin bound to actin filaments undergoes a large structural change (30−35 Å) of the lever arm and a small change at the actin-binding interface upon ADP release (*26*). However, because of the lack of a convenient residue or side chain for exogenous labeling, the specific sites of conformational changes at the actomyosin interface are still unknown. Thus, a more sensitive method of studying local conformational changes in the actin-binding interface upon binding to actin and release of ADP is needed to identify the regions of myosin which mediate its affinity for actin during different stages of the contractile cycle.

In the current study, intrinsic tryptophan fluorescence was used to examine changes in the environment of the A- and R-sites in myosin upon binding to actin in the presence of ADP (ADP-bound) or in the absence of nucleotide (rigor). This was accomplished by generating two mutants of smooth muscle myosin motor domain with the essential light chain (MDE), each containing a single tryptophan residue. The first of these contained the naturally occurring Trp-546 in the A-site (W546-MDE) described previously (*17*), and another mutant had a single nonendogenous tryptophan, substituted for valine 413, located in the R-site (V413W-MDE). Intrinsic tryptophan fluorescence of W546-MDE and V413W-MDE was first used to examine the structural environment of Trp-546 and Trp-413 in the absence of actin. These residues were then monitored in the presence of actin in the ADP-bound and rigor complexes to examine the environment of Trp-546 and Trp-413 in these two strongly bound states. Thus, using a variety of biochemical and fluorescence techniques, we demonstrate that structural changes occur in the A- and R-sites upon binding actin in the ADP-bound and rigor complexes, providing new insights into the mechanism of the actomyosin interaction.

MATERIALS AND METHODS

cDNA Construction. We performed site-directed mutagenesis on a clone of smooth muscle myosin heavy chain containing the motor domain and essential light chain-binding region (residues 1−819, provided by Kathleen Trybus, University of Vermont) to produce two mutants, each containing a single tryptophan residue. Construction of the first mutant containing a single tryptophan residue (546) in the A-site (W546-MDE) by conservative substitution of six of the seven endogenous MDE tryptophans (highlighted in orange in Figure 1) was described previously (*17*). This work also described a mutant containing no tryptophans (Null-MDE, in which Trp-546 was replaced with methionine, highlighted in purple) and one containing all seven native tryptophans (WT-MDE). The second mutant used here, containing a single tryptophan residue (413) in the R-site, was constructed by replacing valine 413 with tryptophan (highlighted in red) in the Null-MDE construct. Valine 413 was a logical site to substitute a tryptophan within the R-site because the corresponding residue is a phenylalanine in skeletal muscle myosin and is a tryptophan in yeast myosin II and *Acanthamoeba* myosin I. The FLAG epitope sequence (DYKDDDK) was added as a fusion tag at the C-terminus of all MDE constructs for purification purposes (*27*).

Protein Expression and Purification. The baculovirus system was used to express all MDE constructs by coinfecting Sf9 insect cells with recombinant baculoviruses encoding the truncated myosin heavy chain and essential light chain. Following incubation with baculoviruses for 3 days, the Sf9 cells were lysed, ammonium sulfate fractionated, and

[1] Abbreviations: DHNBS, dimethyl(2-hydroxy-5-nitrobenzyl)sulfonium bromide; FHC, familial hypertrophic cardiomyopathy; MDE, motor domain essential light chain; Trp or W, tryptophan.

dialyzed overnight in an imidazole-containing buffer (10 mM imidazole-HCl, 90 mM NaCl, 1 mM EGTA, 1 mM NaN_3, 1 mM DTT, pH 7.4) at 4 °C. The dialyzate was bound to an anti-FLAG antibody column and eluted with the homologous peptide. Subsequently, the MDE eluted from the column was pelleted with actin, released in the presence of ATP, and dialyzed overnight into Mops buffer (20 mM Mops, 20 mM KCl, 2 mM $MgCl_2$, 1 mM EGTA, 1 mM DTT, 1 mM NaN_3, pH 7.4). The degree of purity of the MDE was assessed by SDS−PAGE (*28*) using Coomassie-stained gels. Purified MDE concentrations were determined by the method of Bradford (*29*) using the Bio-Rad microplate assay.

Actin was purified from chicken pectoralis muscle using an acetone powder method described previously (*30*) and was polymerized in the presence of phalloidin for actin-pelleting and cosedimentation assays (*31*). The concentration of purified actin was determined spectophotometrically using an extinction coefficient of 0.62 $(mg/mL)^{-1}\cdot cm^{-1}$ at 290 nm.

Actin-Activated ATPase and Actin Cosedimentation Assays. Actin-activated ATPase assays were performed at 37 °C in low ionic strength Mops buffer using a method described previously (*17*). Purified MDE was assayed at a concentration of 0.1 mg/mL in the presence of various actin concentrations (0, 10, 30, 50, 70, and 90 μM) for 70 min (time points taken every 10 min), and inorganic phosphate production was measured colormetrically (*32*). The average ATPase rates [nmol of $P_i\cdot$(nmol of MDE)$^{-1}\cdot s^{-1}$] of three separate preparations of W546-, V413W-, and WT-MDE were plotted as a function of actin concentration and fit with a nonlinear least-squares method. Values of V_{max} and K_M were determined using Michaelis−Menten kinetics.

Actin cosedimentation assays were performed as described previously (*17*). First, MDE was incubated with a 4-fold molar excess of actin in Mops buffer for 30 min on ice and then centrifuged at 95 000 rpm for 30 min in a Beckman TLA 120.2 rotor. The supernatant was removed and the pellet was resuspended in a volume of SDS sample buffer equal to the supernatant. Equal volume samples of the pellet, supernatant, and the MDE−actin complex prior to centrifugation were subjected to SDS−PAGE. Assay results were assessed by visual inspection of the amount of MDE in the supernatant and pellet relative to the amount prior to centrifugation.

Electron Microscopy. The overall conformation of W546- and V413W-MDE bound to actin in a rigor complex was examined by decorating F-actin with these mutants on the grid (*33*) or at approximately stoichiometric ratios in solution (*34*) in Pipes buffer (20−100 mM NaCl, 5 mM NaH_2PO_4, 3 mM $MgCl_2$, 1 mM EGTA, 3 mM NaN_3, 5 mM Pipes, pH 7.0). Grids were negatively stained with 1% uranyl acetate. Filaments were photographed on stain films over holes in the carbon support (*33*) or on thin carbon over holes (*35*). Micrographs were recorded at 52000× on a Philips CM10 electron microscope.

Fluorescence Measurements. A Quantmaster fluorometer (Photon Technology International, South Brunswick, NJ) equipped with a 75-W xenon arc lamp as an excitation source, excitation/emission monochromators, and a WG-320 cutoff emission filter was used to measure steady-state fluorescence. Emission spectra were measured by exciting the sample at 295 nm and collecting the emitted fluorescence from 305 to 400 nm. Quantum yields (Φ) were calculated with a comparative method (*36*) using L-tryptophan as a standard ($\Phi = 0.14$) (*37*).

The fluorescence emission spectra of W546- and V413W-MDE were measured in the absence of actin, as well as in the presence of actin under rigor or ADP-bound (2 mM MgADP) conditions. To obtain the actin-bound spectra of these mutants (MDE−actin ± MgADP), we first collected the data of 3−4 μM actin alone (in the presence or absence of 2 mM MgADP), then added 0.5 μM W546- or V413W-MDE to the actin sample, and collected the MDE−actin spectra. The contribution of actin fluorescence in the MDE−actin spectra, which was 80−85% of the total fluorescence (data not shown), was subtracted using the actin-alone spectra after correction for dilution and inner filter effects. Control experiments using the Null-MDE mutant bound to actin in the rigor and ADP-bound complexes demonstrated that the actin fluorescence was unaffected by MDE binding as reported previously (*17*). In addition, previous results obtained with the W625-MDE mutant, which contains a single native tryptophan at residue 625, demonstrated that the W625-MDE spectrum in the presence of actin, obtained by subtracting the actin-alone spectrum, was nearly identical to the spectrum in the absence of actin (*17*). This provides evidence that our method of subtracting the actin fluorescence was reliable. The average rigor and ADP-bound spectra and maximum emission wavelength (λ_{max}) of W546- and V413W-MDE were obtained by averaging at least three independent experiments.

A Timemaster time-resolved fluorometer (Photon Technology International) equipped with a N_2 flash lamp and gated photomultiplier tube was used to determine the fluorescence lifetime of the MDE mutants. Samples were excited at 297 nm, and the time-resolved emission decay was collected at λ_{max} (determined from the steady-state emission spectra). Time-resolved emission decays were deconvoluted to determine the fluorescence lifetimes using proprietary software from Photon Technology International.

Acrylamide quenching was used to determine the degree of exposure to solvent of Trp-546 and -413 in solution. The decrease in fluorescence intensity at λ_{max} was measured as a function of increasing acrylamide concentrations ([Q]). The fluorescence intensity in the absence of quencher (F_0) divided by the fluorescence intensity in the presence of quencher (F) was used to quantify the relative change in fluorescence resulting from acrylamide quenching (F_0/F). F_0/F was plotted as a function of [Q] and fit to the Stern−Volmer relationship, taking into account both static (V) and dynamic quenching (K_{SV}) constants: $F_0/F = (1 + K_{SV}[Q])\exp(V[Q])$ (*38*). In addition, the bimolecular quenching constant (k_q) was calculated by dividing K_{SV} by the fluorescence lifetime (τ).

Dimethyl(2-hydroxy-5-nitrobenzyl)sulfonium bromide (DHNBS) was used to selectively oxidize the single tryptophan residues in W546- and V413W-MDE bound to actin in ADP-bound and rigor conditions. Following incubation of 2 μM MDE with 10 μM actin for 30 min on ice, a 20-fold molar excess of DHNBS was added and incubated for 10 min. Excess DHNBS was then quenched by the addition of 5 mM DTT. The MDE bound to actin was pelleted as described above, the supernatant removed, and the pellet resuspended in Mops buffer with 2 mM MgATP. Subsequent centrifugation was used to separate the unbound MDE from actin. The degree of DHNBS quenching was determined from the

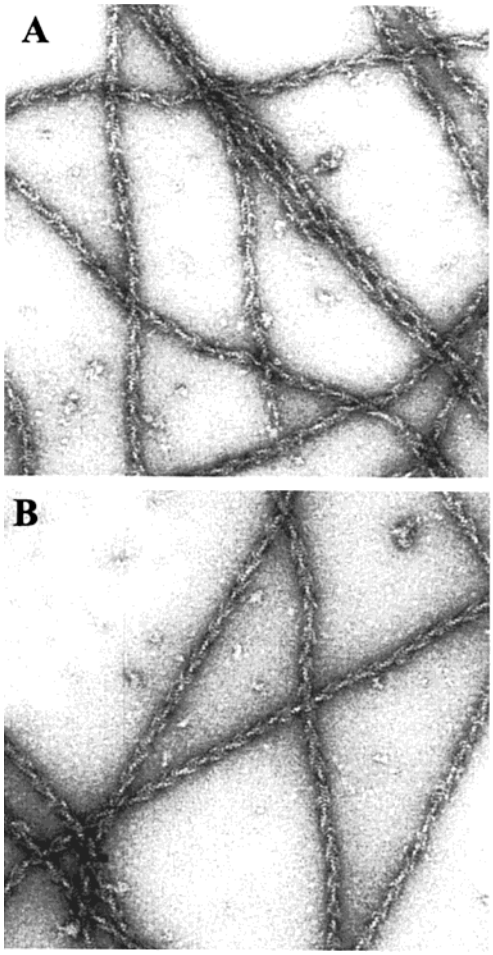

FIGURE 2: Electron micrographs of W546- and V413W-MDE decorated actin filaments. MDE (0.2 mg/mL) was applied to actin (0.05 mg/mL) spread on carbon holey triafol removed grids and stained with uranyl acetate. The grids were viewed using a Phillips CM10 electron microscope, and micrographs were taken at 52000× (reproduced at 80% of original size).

steady-state fluorescence emission spectra of the MDE released from actin after the spectra were corrected for differences in concentration. Also, samples of the pellet, supernatant, and released MDE were subjected to SDS−PAGE to ensure that actin binding was unaffected by the presence of DHNBS.

RESULTS

Functional Assays. A series of functional assays were performed to examine the impact of the conservative mutations made to generate the smooth muscle myosin single tryptophan-containing mutants, W546- and V413W-MDE, in comparison to WT-MDE. MDE constructs were expressed and purified (90−95%) with similar yields of approximately 1−2 mg per 1×10^9 Sf9 cells. Both W546- and V413W-MDE decorate actin with the classic arrowhead appearance (*33*−*35*, *39*) as shown in electron micrographs (Figure 2). In addition, we examined the ability of the MDE constructs to bind actin in the presence (ADP-bound) and absence (rigor) of 2 mM MgADP with actin cosedimentation assays. As shown in Figure 3, our analysis demonstrated that essentially all of the W546- and V413W-MDE was bound to actin under both ADP-bound and rigor conditions and thus was present in the pellet following sedimentation. Also,

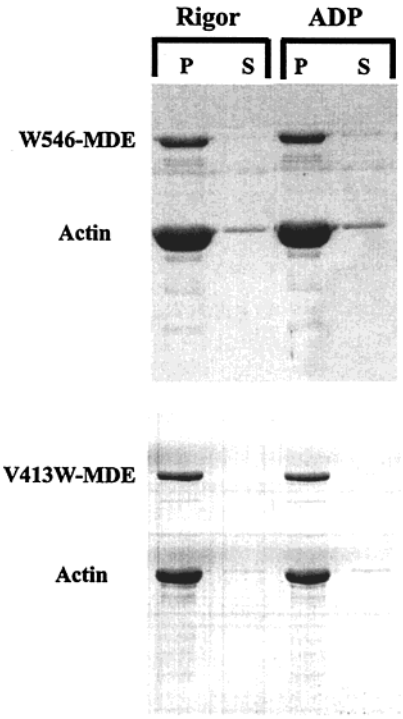

FIGURE 3: Actin cosedimentation assays of W546- and V413W-MDE in the presence of 2 mM MgADP (ADP-bound) and absence of nucleotide (rigor). Equal volume samples were subjected to SDS−PAGE to assess the amount of MDE bound to actin in the pellet (P) relative to the amount in the supernatant (S) following centrifugation. When MDE was centrifuged in the absence of actin, all of the protein remained in the supernatant (data not shown).

Table 1: Summary of Low-Salt (20 mM KCl) Actin-Activated ATPase Data[a]

MDE mutant	rate at 30 μM actin (s^{-1})	V_{max} (s^{-1})	K_M (μM)	V_{max}/K_M ($s^{-1}\cdot\mu M^{-1}$)
WT-MDE	0.18 ± 0.05[b]	0.76	62	1.2×10^{-2}
W546-MDE	0.09 ± 0.01[b]	0.36	99	3.6×10^{-3}
V413W-MDE	0.08 ± 0.01[b]	0.20	49	4.0×10^{-3}

[a] V_{max} and K_M values were calculated by plotting ATPase rates [nmol of P_i·(nmol of MDE)$^{-1}$·s^{-1}] from two to three different preparations of each MDE construct as a function of actin concentration (10, 30, 50, 70, 90 μM) and fitting the curves to Michaelis−Menten kinetics. [b] ATPase rates are given as the mean ± standard error.

preliminary experiments have demonstrated that the binding of WT- and Null-MDE to yeast actin, which has a lower affinity for vertebrate muscle myosin than does vertebrate muscle actin, was virtually identical in a rigor complex (Emil Reisler, personal communication).

Finally, steady-state ATPase assays demonstrated that the V_{max} of W546- and V413W-MDE was reduced 2−4-fold, while their K_M values were within 40% of WT-MDE, and their total activity (V_{max}/K_M) was 30−35% of WT-MDE (Table 1). Thus, the results of our functional assays indicate that both W546- and V413W-MDE bind actin normally and, although 65−70% compromised, have retained their ability to hydrolyze ATP in an actin-dependent manner.

Fluorescence Properties in the Absence of Actin. The structural environment of Trp-546 and Trp-413 was probed by examining the steady-state and time-resolved fluorescence properties of W546- and V413W-MDE (summarized in Table 2). The steady-state fluorescence emission spectra indicated that W546- and V413W-MDE exhibit emission

Table 2: Fluorescence Properties of W546- and V413W-MDE[a]

MDE mutant	λ_{max} (nm)	Φ	τ (ns)	K_{SV} (M^{-1})	V (M^{-1})	k_q (M^{-1}·ns^{-1})
546-MDE	344	0.20	1.8 ± 0.16[b]	11.5 ± 0.23[c]	2.0	6.4 ± 0.7[d]
V413W-MDE	338	0.27	2.2 ± 0.04[b]	8.0 ± 0.20[c]	2.0	3.6 ± 0.1[d]

[a] Emission peak maximum (λ_{max}) and quantum yield (Φ) were determined from the steady-state fluorescence spectrum. [b] The average lifetime (τ) was determined from the time-resolved fluorescence decay ($\pm$ standard error). [c] Dynamic (K_{SV}) ($\pm$ standard error) and static (V) acrylamide quenching constants were calculated using the Stern−Volmer relationship (see Materials and Methods). [d] The bimolecular (k_q) ($\pm$ relative error) acrylamide quenching constant was calculated by normalizing K_{SV} by the fluorescence lifetime (τ) (see Materials and Methods).

maxima (λ_{max}) of 344 and 338 nm, respectively (Figure 4), and quantum yields (Φ) of 0.20 and 0.27. Time-resolved fluorescence measurements of the two MDE mutants demonstrated an average lifetime (τ) of 1.8 ns for W546-MDE and 2.2 ns for V413W-MDE. These results indicate that both Trp-546 and Trp-413 are in a polar environment with Trp-546 slightly more so, perhaps due to greater solvent accessibility.

To specifically examine the degree of solvent exposure of Trp-546 and Trp-413 in the absence of actin, we performed acrylamide quenching experiments on W546- and V413W-MDE (summarized in Table 2). The Stern−Volmer relationship was used to quantitatively determine the accessibility to solvent. The dynamic quenching constants (K_{SV}), defined by the quenching that occurs by interaction of acrylamide with the tryptophan in its excited state, were calculated to be 11.5 and 8 M^{-1} for W546- and V413W-MDE, respectively. In addition, the bimolecular quenching constants (k_q) for W546- and V413W-MDE, in which the dynamic quenching is normalized by the fluorescence lifetime, were calculated to be 6.4 M^{-1}·ns^{-1} and 3.6 M^{-1}·ns^{-1}, respectively. Given that the k_q values determined for solvent-exposed tryptophans in proteins are approximately 4.0 M^{-1}·ns^{-1} (*38*), these results indicate that both Trp-546 and Trp-413 are quite solvent exposed. It is likely that Trp-546 is slightly more exposed to solvent than Trp-413, which is in agreement with the small differences observed in the λ_{max} and quantum yield.

Fluorescence Properties in the Presence of Actin. We examined the changes in the environment of Trp-546 and Trp-413 complexed with actin in two strongly bound states (ADP-bound and rigor). Figure 5 demonstrates the fluorescence spectra of W546- and V413W-MDE bound to actin in the presence of 2 mM MgADP or in rigor, following subtraction of the intrinsic actin fluorescence (see Materials and Methods). The average spectrum of W546-MDE is blue-shifted with a λ_{max} of 337 ($\pm$2.0) nm in the ADP-bound complex and 336 ($\pm$1.0) nm in the rigor complex, indicating that Trp-546 adopts a less polar conformation in the ADP-bound and rigor complexes than in the absence of actin. Interestingly, V413W-MDE has a λ_{max} of 338 ($\pm$0.8) nm in the ADP-bound complex, similar to the unbound spectrum. However, V413W-MDE exhibits several possible λ_{max}'s in the rigor complex, which range from a more polar environment (i.e., rigor 1, $\lambda_{max} = 347 \pm 1.1$ nm) to an environment similar to that found in the ADP-bound complex (i.e., rigor 2, $\lambda_{max} = 341 \pm 0.6$ nm). Thus, while Trp-546 is in a less polar environment in both strongly bound states, Trp-413 has a single conformation in the ADP-bound state and in the rigor complex can adopt several conformations that are in a more polar environment.

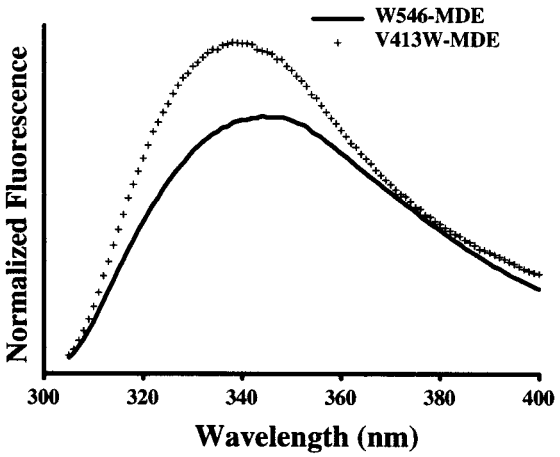

FIGURE 4: Steady-state fluorescence emission spectra of W546- and V413W-MDE (excitation wavelength of 295 nm) collected from 300 to 400 nm. The quantum yields and emission peak maxima are shown in Table 2.

To determine the exposure to solvent of Trp-546 and Trp-413 in the ADP-bound and rigor actomyosin complexes, we used a permanent quencher (DHNBS) to oxidize Trp-546 and Trp-413 in the presence of actin, under ADP-bound and rigor conditions. We then measured the resulting steady-state fluorescence after releasing the MDE from actin. The fluorescence spectrum of W546-MDE in the ADP-bound and rigor complexes, indicating the degree of DHNBS quenching, was similar in both complexes with 10% more quenching in the ADP-bound state (Figure 6A). However, V413W-MDE was 50% less quenched in the ADP-bound complex than in the rigor complex (Figure 6B). Thus, the exposure to solvent of Trp-546 is similar in both the ADP-bound and rigor complexes, while Trp-413 is less accessible to solvent in the ADP-bound complex than in the rigor complex. Furthermore, these results are consistent with the steady-state spectral changes observed for W546- and V413W-MDE in the ADP-bound and rigor actomyosin complexes. Overall, these data indicate that Trp-546 in the A-site is buried within the actomyosin interface in both strongly bound states, while Trp-413 in the R-site adopts a more flexible and exposed conformation upon ADP release.

DISCUSSION

To understand how myosin converts the energy of ATP hydrolysis into mechanical work, it is critical to determine the specific nucleotide-dependent conformational changes that occur in the actin-binding region of myosin. We have developed a sensitive method utilizing mutants of smooth muscle myosin containing a single tryptophan in two proposed actin-binding sites, the A-site (W546-MDE) and R-site (V413W-MDE), to identify specific conformational changes that are associated with actin binding in the presence of ADP (ADP-bound) or absence of nucleotide (rigor). These results suggest a structural model that explains how specific conformational changes in the A-site and R-site may mediate myosin's affinity for actin throughout the contractile cycle.

Structure and Function of W546- and V413-MDE. Several functional assays were performed to determine how the conservative substitutions made in the W546- and V413W-

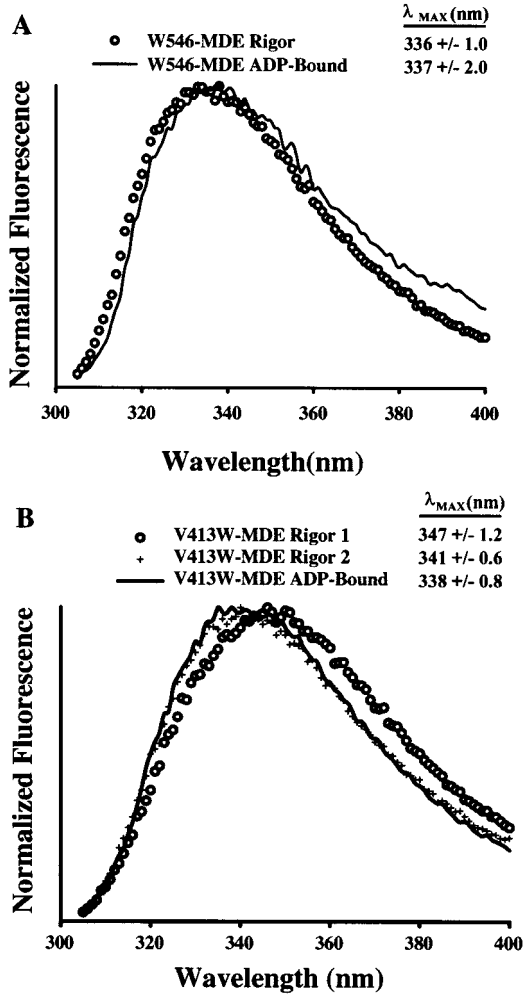

FIGURE 5: Actin-induced shifts in the steady-state fluorescence emission spectra of W546- and V413W-MDE in the ADP-bound as well as rigor actomyosin complexes. Spectra are the calculated average of at least three independent experiments with the maximum emission wavelength average (± standard error) shown in the legend. (A) The fluorescence emission spectrum of W546-MDE blue-shifts (λ_{max}) from 344 to 337 nm upon binding to actin in the ADP-bound complex and is similar in the rigor actomyosin complex (λ_{max} = 336 nm). (B) The fluorescence emission spectrum of V413W-MDE contains an emission peak maximum of 338 nm in the ADP-bound actomyosin complex, and in the rigor complex a range of red-shifted emission spectra are observed (λ_{max} = 341−347 nm).

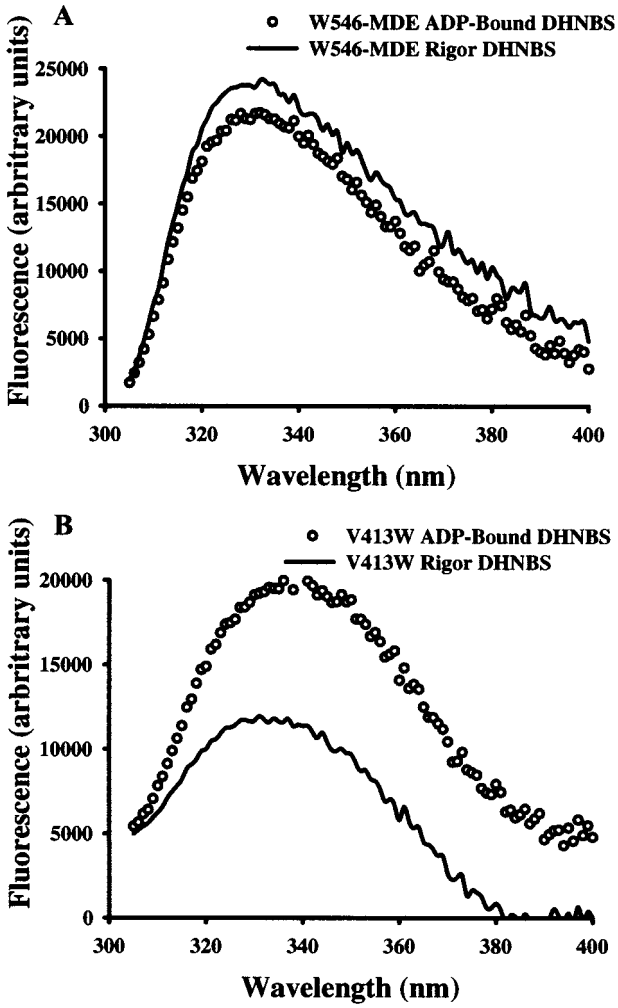

FIGURE 6: DHNBS quenching of W546- and V413W-MDE in the ADP-bound complex compared to the rigor actomyosin complex. V413W-MDE (2.5 μM) complexed with actin (10 μM) was reacted with a 20-fold molar excess of DHNBS (50 μM) for 15 min in the presence and absence of 2 mM MgADP. The actomyosin complex was pelleted subsequently released with MgATP, and the protein concentration normalized steady-state fluorescence emission was measured. W546-MDE was 10% more quenched in the ADP-bound complex compared to the rigor actomyosin complex, whereas V413W-MDE was 50% more quenched in the rigor complex than in the ADP-bound actomyosin complex.

MDE mutants affected the native properties of myosin. Although the actin-activated ATPase activities of W546- and V413W-MDE were reduced by 65−70%, their ability to bind actin was similar to that of WT-MDE. Five of the substitutions made in these constructs were to residues that occur at equivalent positions in other myosin isoforms (W29F, W36F, V413W, W54M, and W625F) and would not be expected to significantly alter the enzymatic properties of MDE. Thus, we feel it is most likely that the substitutions made at one or more of the three tryptophans in MDE which are conserved among myosins (residues W441F, W512F, and W597F) may have resulted in the observed changes in enzymatic activity. However, these three conserved tryptophans are not located near the actin-binding region and were substituted conservatively with phenylalanine. Since W546- and V413W-MDE are capable of binding actin in a strongly bound complex, and the hydrolysis of ATP is activated in the presence of actin, we conclude that they are extremely useful in probing the structural properties of the actomyosin interface in the ADP-bound and rigor complexes.

The steady-state fluorescence emission spectra maxima, quantum yields, and acrylamide quenching of W546- and V413W-MDE demonstrate that both Trp-546 and Trp-413 are highly exposed to solvent (Table 2), similar to the observed conformation of these residues in the crystal structure of MDE (*1*). In addition, the fluorescence profile of Trp-546 demonstrated that it is in a more polar environment than Trp-413, perhaps because Trp-546 is more solvent exposed. However, despite the large difference in the measured bimolecular quenching constants (k_q), this difference in the solvent accessibility of Trp-546 and Trp-413 is likely to be exaggerated. A considerable amount of error, due to the difficulty in measuring the lifetime of W546-MDE, which has a relatively low quantum yield, may have contributed to the high k_q value measured for W546-MDE.

Alternatively, although not shown in the crystal structure, Trp-413 may interact with an adjacent part of myosin in solution, which would explain its fluorescence profile that indicates it is less solvent exposed than Trp-546. Despite these uncertainties as to the exact degree of solvent exposure of Trp-546 compared to Trp-413, we feel that the data for each mutant in the absence of actin can accurately be compared to its properties in the presence of actin. These comparisons have allowed us to better understand the relative contributions of these two sites to the progressive changes in actin affinity which occur throughout the contractile cycle.

Role of the A-Site and R-Site in Binding Actin. Results from cryo-EM (*11*, *12*) as well as mutagenesis studies (*40*) have predicted that the A-site may be one of the primary points of contact with actin in the strongly bound actomyosin complexes. As reported previously (*17*), Trp-546 adopts a more buried conformation in both strongly bound actomyosin complexes, ADP-bound and rigor, compared to W546-MDE alone. This is apparent from the 7−8 nm blue shift (344 → 337−336) in the emission spectrum maximum and the protection from DHNBS oxidation in the ADP-bound and rigor complexes. Interestingly, upon ADP release Trp-546 adopts a slightly more buried conformation as indicated by a blue-shift in the shape of the emission spectrum and a small increase (10%) in protection from DHNBS quenching. Together, these results suggest that the A-site interacts with actin in both strongly bound actomyosin complexes and that ADP release may result in a small conformation change in the A-site, perhaps due to a tighter interaction with actin.

Several independent studies have provided evidence that the R-site may be important for mediating the actin-activated ATPase rate and actomyosin affinity. Synthetic peptides of the R-site have been shown to decrease the actin-activated ATPase rate of skeletal muscle myosin without changing K_M (*19*). Furthermore, biophysical and biochemical characterization of the R-site loop Arg403Glu mutation in cardiac myosin, which is associated with the disease FHC, demonstrated that this mutation affects the actin-activated ATPase V_{max} and K_M values (*41*−*44*). In addition, velocity in the in vitro motility assay, as well as the amount of time myosin remains strongly bound to actin, was affected by the Arg403Glu mutation (*45*). These studies suggest that the R-site may mediate actin affinity by regulating the amount of time myosin remains strongly bound to actin, perhaps through changing its conformation following P_i release, which limits the actin-activated ATPase rate (*46*), and/or following ADP release, which limits unloaded shortening velocity (*47*).

Our measurements of the fluorescence properties of V413W-MDE bound to actin suggest that the R-site, unlike the A-site, undergoes a large conformational change upon ADP release. In the ADP-bound complex Trp-413 adopts a buried conformation, as indicated by its protection from DHNBS oxidation in the ADP-bound complex compared to the absence of actin (data not shown), suggesting that Trp-413 may interact with actin in the ADP-bound complex. In contrast, the emission spectra and DHNBS oxidation experiments of V413W-MDE bound to actin in rigor indicate that the R-site adopts a more flexible and solvent-exposed conformation upon ADP release. This flexibility is demonstrated by a range of emission spectra in the rigor complex containing red-shifted emission maxima (341−347 nm),

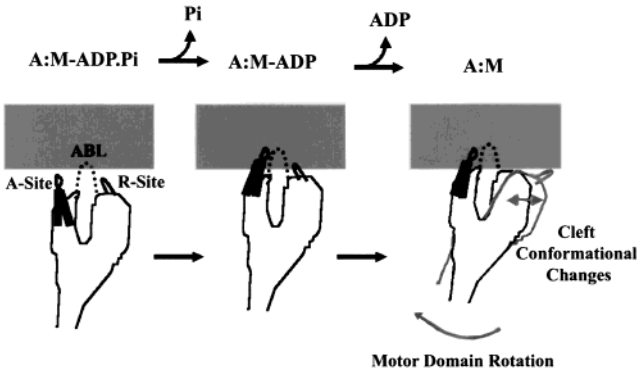

FIGURE 7: Model of structural interactions at the actomyosin interface leading from weakly to strongly bound complexes. The role of the ABL (dotted line) is shown as the main interaction in the presence of ADP·P_i (A−M:ADP·P_i). The release of P_i (A−M:ADP) results in the A-site (helix−loop−helix) and R-site (solid line) forming contacts with actin. Finally, ADP release results in formation of the rigor complex (A−M) due to a stable interaction of the A-site with actin (i.e., Trp-546 remains in a buried environment) and increased flexibility of the R-site (i.e., Trp-413 adopts a more flexible exposed conformation). Global conformational changes such as opening/closing of the actin-binding cleft and/or rotation of the entire motor domain may result in the local conformational changes observed at the A- and R-sites.

which suggests that Trp-413 can adopt several specific conformations in the rigor complex. Furthermore, DHNBS oxidation demonstrated that Trp-413 is 50% more accessible to solvent in the rigor complex than in the ADP-bound complex. Cryo-EM performed on smooth muscle myosin bound to actin has shown a large change in the lever arm region and a small change in the actin-binding region upon ADP release (*26*). Given our results, we suggest that at least part of the change at the actomyosin interface observed by cryo-EM is a movement of the R-site. In addition, our results imply that the structural rearrangements that occur in the actomyosin complex upon ADP release involve communication over the large distance between the active site and R-site. The movement of the R-site may be important for mediating the 5−6-fold (*48*) increase in the affinity of myosin for actin observed upon ADP release.

Structural Model of the Actomyosin Interaction. Two global conformational changes have been postulated to explain how myosin may mediate its affinity for actin during the contractile cycle. One set of predictions suggests that the actin-binding cleft becomes more open or closed, altering the interface between actin and myosin (*49*, *50*). Crystallographic results obtained from *Dictyostelium* (*51*), smooth muscle (*1*), and scallop myosin (*6*) support conformational changes around the cleft, but it is still unclear how these movements may occur in the presence of actin. These nucleotide-induced conformational changes in the actin-binding cleft demonstrated crystallographically have been shown as rotations of the lower 50 kDa subdomain relative to the rest of the motor domain. However, since our results indicate that the lower 50 kDa subdomain A-site interacts with actin in both strongly bound states, it is likely that conformational changes around the actin-binding cleft result in rotation of the rest of the motor domain relative to the lower 50 kDa subdomain A-site and actin. A second proposal is that the entire motor domain rotates as a rigid body during the contractile cycle, demonstrated by cryo-EM of *Drosophila* indirect flight muscle (*52*). Regardless of their exact

nature, these global structural changes must lead to more localized conformational changes at the actomyosin interface that are ultimately responsible for altering the affinity between actin and myosin.

We have developed a structural model to explain the sequential steps of the actomyosin interaction leading from weak to strong binding (Figure 7), which takes into account the current results as well as those already established in the literature. First, the ABL forms a weak interaction with actin while ATP and ADP−P_i are bound to the active site (*13*−*16*). Following P_i release from the active site, myosin dramatically increases its affinity for actin by incorporating both the A-site (purple) and the R-site (red) into the actomyosin interface. The release of P_i is also thought to correlate with rotation of the lever arm and force production. Once ADP, the final product of ATP hydrolysis, is released from the active site, the R-site is no longer stabilized by the contents of the active site and is free to alter its conformation, whereas the A-site remains tightly bound to actin. The shift in conformation of the R-site may remove a steric block by the loop, leading to more contacts of the upper 50 kDa subdomain of myosin with actin in the rigor complex. Alternatively, a part of the R-site loop, containing Trp-413, may interact with actin in the ADP-bound complex, and upon ADP release another part of the loop, or the upper 50 kDa subdomain, may interact with actin, causing Trp-413 to become more flexible and solvent exposed. It is likely that global conformational changes, including rotation of the motor domain and/or changes in the actin-binding cleft, underlie the changes in the local environment we have observed at the actin-binding interface upon ADP release. Overall, our results suggest that the A-site is the primary contact between actin and myosin in the strongly bound states, while the R-site shifts its conformation during ADP release allowing formation of the rigor complex.

In summary, we have used intrinsic tryptophan fluorescence to measure local conformational changes in two important actin-binding regions of myosin and to examine the dynamic properties of these sites in the presence of actin. We provide evidence that the lower 50 kDa subdomain A-site binds tightly to actin in both strongly bound states (ADP-bound and rigor), suggesting that it functions as the main contact between actin and myosin during these states. In addition, we suggest that the upper 50 kDa subdomain R-site functions mainly to stabilize interactions with actin in the ADP-bound complex and alter its conformation upon ADP release to promote formation of the higher affinity rigor complex. We have established a model based on our results as well as previous studies that can be tested in future experiments to further examine the global and local conformational changes that mediate myosin's affinity for actin.

ACKNOWLEDGMENT

We thank Dr. Roger Craig (University of Massachusetts Medical Center) for performing the electron micrographs and for helpful discussions. We also thank the University of Vermont Muscle Club for many stimulating conversations and suggestions.

REFERENCES

1. Dominguez, R., Freyzon, Y., Trybus, K. M., and Cohen, C. (1998) *Cell 94*, 559−571.
2. Fisher, A. J., Smith, C. A., Thoden, J. B., Smith, R., Sutoh, K., Holden, H. M., and Rayment, I. (1995) *Biochemistry 34*, 8960−8972.
3. Rayment, I., Rypniewski, W. R., Schmidt-Base, K., Smith, R., Tomchick, D. R., Benning, M. M., Winkelmann, D. A., Wesenberg, G., and Holden, H. M. (1993) *Science 261*, 50−58.
4. Smith, C. A., and Rayment, I. (1995) *Biochemistry 34*, 8973−8981.
5. Smith, C. A., and Rayment, I. (1996) *Biochemistry 35*, 5404−5417.
6. Houdusse, A., Kalabokis, V. N., Himmel, D., Szent-Gyorgyi, A. G., and Cohen, C. (1999) *Cell 97*, 459−470.
7. Kabsch, W., Mannherz, H. G., Suck, D., Pai, E. F., and Holmes, K. C. (1990) *Nature 347*, 37−44.
8. McLaughlin, P. J., Gooch, J. T., Mannherz, H. G., and Weeds, A. G. (1993) *Nature 364*, 685−692.
9. Schutt, C. E., Myslik, J. C., Rozycki, M. D., Goonesekere, N. C., and Lindberg, U. (1993) *Nature 365*, 810−816.
10. Lorenz, M., Popp, D., and Holmes, K. C. (1993) *J. Mol. Biol. 234*, 826−836.
11. Milligan, R. A. (1996) *Proc. Natl. Acad. Sci. U.S.A. 93*, 21−26.
12. Rayment, I., Holden, H. M., Whittaker, M., Yohn, C. B., Lorenz, M., Holmes, K. C., and Milligan, R. A. (1993) *Science 261*, 58−65.
13. Sutoh, K. (1982) *Biochemistry 21*, 4800−4804.
14. Mornet, D., Bertrand, R. U., Pantel, P., Audemard, E., and Kassab, R. (1981) *Biochemistry 20*, 2110−2120.
15. Rovner, A. S., Freyzon, Y., and Trybus, K. M. (1995) *J. Biol. Chem. 270*, 30260−30263.
16. Yamamoto, K. (1991) *J. Mol. Biol. 217*, 229−233.
17. Yengo, C. M., Fagnant, P. M., Chrin, L., Rovner, A. S., and Berger, C. L. (1998) *Proc. Natl. Acad. Sci. U.S.A. 95*, 12944−12949.
18. Geisterfer-Lowrance, A. A., Kass, S., Tanigawa, G., Vosberg, H. P., McKenna, W., Seidman, C. E., and Seidman, J. G. (1990) *Cell 62*, 999−1006.
19. Bartegi, A., Roustan, C., Chavanieu, A., Kassab, R., and Fattoum, A. (1997) *Eur. J. Biochem. 250*, 484−491.
20. Bement, W. M., and Mooseker, M. S. (1995) *Cell Motil. Cytoskeleton 31*, 87−92.
21. Brzeska, H., and Korn, E. D. (1996) *J. Biol. Chem. 271*, 16983−16986.
22. Goldman, Y. E. (1998) *Cell 93*, 1−4.
23. Baker, J. E., Brust-Mascher, I., Ramachandran, S., LaConte, L. E., and Thomas, D. D. (1998) *Proc. Natl. Acad. Sci. U.S.A. 95*, 2944−2949.
24. Berger, C. L., and Thomas, D. D. (1993) *Biochemistry 32*, 3812−3821.
25. Berger, C. L., and Thomas, D. D. (1994) *Biophys. J. 67*, 250−261.
26. Whittaker, M., Wilson-Kubalek, E. M., Smith, J. E., Faust, L., Milligan, R. A., and Sweeney, H. L. (1995) *Nature 378*, 748−751.
27. Brizzard, B. L., Chubet, R. G., and Vizard, D. L. (1994) *BioTechniques 16*, 730−734.
28. Laemmli, U. K. (1970) *Nature 227*, 680−685.
29. Bradford, M. M. (1976) *Anal. Biochem. 72*, 248−254.
30. Pardee, J. D., and Spudich, J. A. (1982) *Methods Enzymol. 85*, 164−181.
31. Dancker, P., Low, I., Hasselbach, W., and Weiland, T. H. (1975) *Biochim. Biophys. Acta 400*, 407−414.
32. White, H. D. (1982) *Methods Enzymol. 85*, 698−708.
33. Craig, R., Szent-Gyorgyi, A. G., Beese, L., Flicker, P., Vibert, P., and Cohen, C. (1980) *J. Mol. Biol. 140*, 35−55.
34. Frado, L. L., and Craig, R. (1992), *J. Mol. Biol. 223*, 391−397.
35. Moody, C., Lehman, W., and Craig, R. (1990) *J. Muscle Res. Cell Motil. 11*, 176−185
36. Parker, C. A., and Reese, W. T. (1960) *Analyst 85*, 587−600.
37. Valeur, B., and Weber, G. (1977) *Photochem. Photobiol. 25*, 441−444.

38. Eftink, M. R., and Ghiron, C. A. (1976) *Biochemistry 15*, 672−680.
39. Huxley, H. (1969) *Science 164*, 1356−1366.
40. Onishi, H., Morales, M. F., Katoh, K., and Fujiwara, K. (1995) *Proc. Natl. Acad. Sci. U.S.A. 92*, 11965−11969.
41. Sweeney, H. L., Straceski, A. J., Leinwand, L. A., Tikunov, B. A., and Faust, L. (1994) *J. Biol. Chem. 269*, 1603−1605.
42. Fujita, H., Sugiura, S., Momomura, S., Omata, M., Sugi, H., and Sutoh, K. (1997) *J. Clin. Invest. 99*, 1010−1015.
43. Roopnarine, O., and Leinwand, L. A. (1998) *Biophys. J. 75*, 3023−3030.
44. Sata, M., and Ikebe, M. (1996) *J. Clin. Invest. 98*, 2866−2873.
45. Tyska, M. J., Hayes, E., Giewat, M., Seidman, C. E., Seidman, J. G., and Warshaw, D. M. (1998) *Biophys. J. 74*, A121.
46. Lymn, R. W., and Taylor, E. W. (1971) *Biochemistry 10*, 4617−4624.
47. Siemankowski, R. F., Wiseman, M. O., and White, H. D. (1985) *Proc. Natl. Acad. Sci. U.S.A. 82*, 658−662.
48. Cremo, C. R., and Geeves, M. A. (1998) *Biochemistry 37*, 1969−1978.
49. Gulick, A. M., and Rayment, I. (1997) *BioEssays 19*, 561−569.
50. Holmes, K. C. (1996) *Curr. Opin. Struct. Biol. 6*, 781−789.
51. Rayment, I. (1996) *J. Biol. Chem. 271*, 15850−15853.
52. Schmitz, H. Reedy, M. C., Reedy, M. K., Tregear, R. T., and Taylor, K. A. (1997) *J. Cell Biol. 139*, 695−707.

BI991226L